analytical chemistry

pubs.acs.org/ac Article

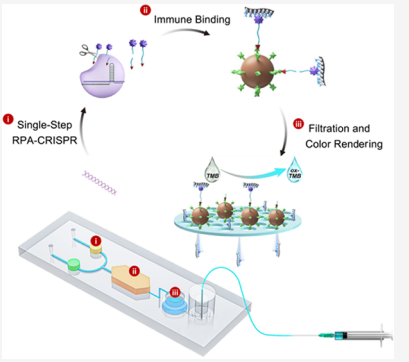
Two-Dimensional Nanozyme-Catalyzed Colorimetric CRISPR Assay for the Microfluidic Detection of Monkeypox Virus

Hong Chen,[#] Xiaodan Cheng,[#] Yunxiang Wang,[#] Ning Han,[#] Liyan Liu, Hongjuan Wei, Zhijie Tu, Zhixia Gu, Rui Song,[*] Shengqi Wang,[*] and Zhen Rong[*]

Cite This: https://doi.org/10.1021/acs.analchem.4c05570 Read Online

ACCESS | Metrics & More | Article Recommendations | Supporting Information

ABSTRACT: The recent monkeypox epidemic outbreaks worldwide highlight the urgent need for fast and precise diagnostic solutions, especially in resource-limited settings. Here, a two-dimensional nanozyme-catalyzed colorimetric CRISPR assay for the microfluidic detection of the monkeypox virus (MPXV) was established. We utilized graphene oxide as a substrate for the adsorption of gold seeds and the deposition of a porous Pt shell to prepare high-performance two-dimensional GO@Pt nanomaterials. The viral nucleic acids released from clinical samples initiated a single-step recombinase polymerase amplification-CRISPR/Cas13a for the trans-cleavage of ssRNA reporters labeled with FAM and biotin. These reporters can be recognized by FAM antibody-conjugated GO@Pt nanozymes and streptavidin-coated magnetic beads. The formed sandwich immunocomplexes can catalyze the oxidation of a colorless 3,3′,5,5′-tetramethylbenzidine substrate with a distinct color change. The proposed GO@Pt-catalyzed colorimetric CRISPR assay exhibited a limit of detection of 1 copy/μL of MPXV in 60 min. Forty clinical samples, including rash fluid swabs and oral swabs, were tested with 100% agreement with the real-time PCR. These results indicate the excellent potential of GO@Pt-catalyzed colorimetric CRISPR for the sensitive and accurate testing of MPXV under resource-constrained conditions.



INTRODUCTION

Since May 20, 2022, the monkeypox epidemic has spread widely in multiple regions worldwide. More than 89000 confirmed cases of monkeypox, including 152 deaths, have been reported in 113 countries and regions. Monkeypox is a viral zoonosis caused by infection with the monkeypox virus (MPXV), a large double-stranded DNA virus (~197 kb) belonging to *Orthopoxvirus*,[1] which behaves similarly to smallpox and is accidentally transmitted to humans upon encountering an infected animal.[2] In recent outbreaks, more than half of the monkeypox cases may have been passed to others before the symptoms appeared, and monkeypox nucleic acid has been detected in anal swabs from asymptomatic infected men. Therefore, developing reliable, fast, and easily accessible detection technologies is vital for the early diagnosis and efficient control of this disease.

Nucleic acid amplification testing is the most reliable and efficient diagnostic method for infectious diseases. The traditional and commonly used experimental methods for MPXV DNA detection mainly include real-time fluorescent polymerase chain reaction (PCR), isothermal amplification, and the emerging clustered regularly interspaced short palindromic repeats (CRISPR)/Cas-associated systems.[3−6] As the gold standard for detecting nucleic acids, PCR has been applied to the detection of MPXV DNA. Despite its high sensitivity and strong specificity, it requires complicated procedures, skilled operators, and precise and expensive equipment.[7] Compared with PCR, isothermal amplification can achieve nucleic acid amplification under specific temperature conditions with sensitivity lower than that of PCR.

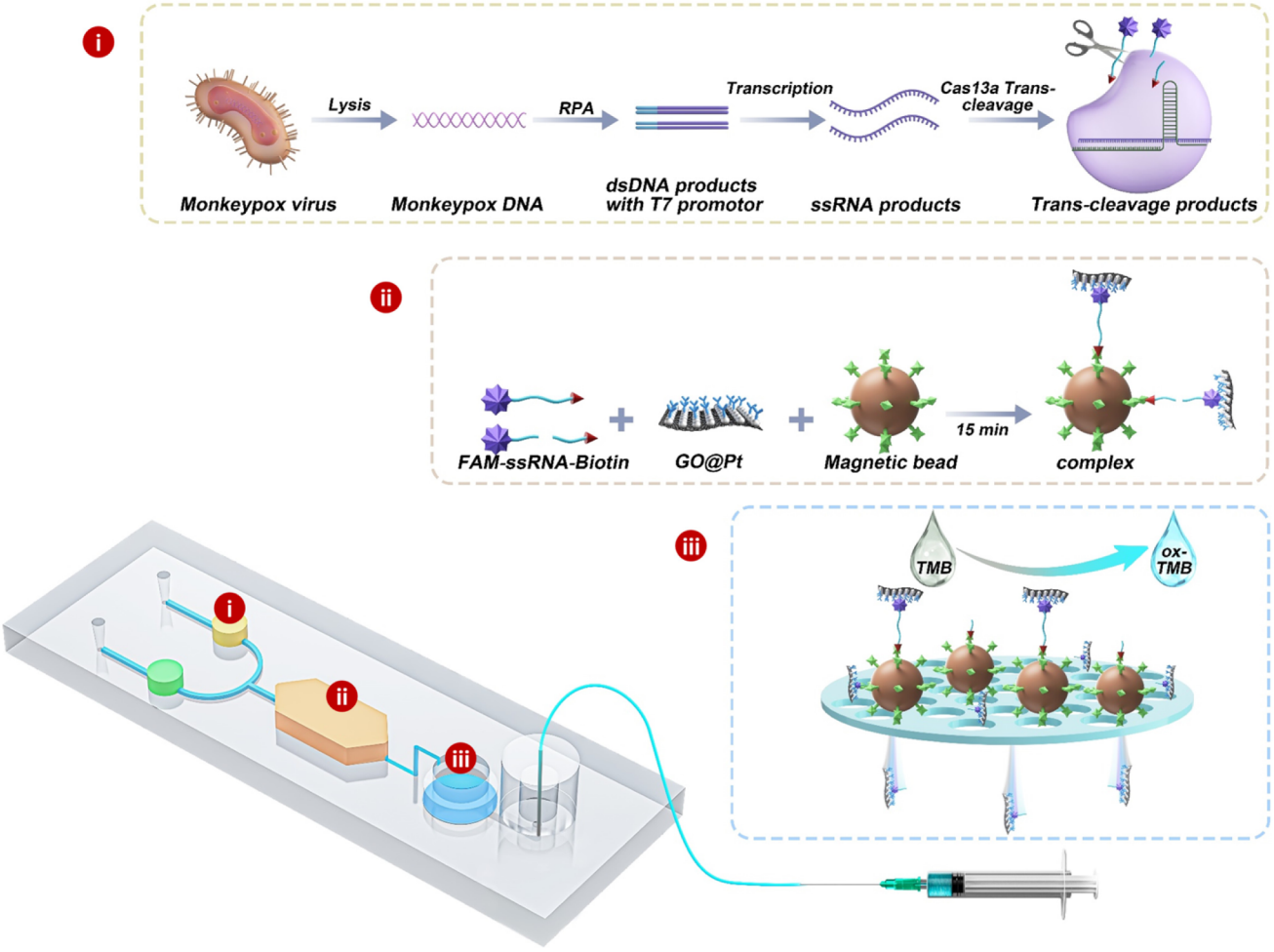
CRISPR/Cas protein diagnostic technology has been widely used in the development and application of point-of-care testing systems because of its fast reaction rate, high sensitivity, and minimal external reaction conditions.[8−11] Recently, CRISPR-based diagnostic methods have been developed for MPXV detection[12,13] The signal readout methods of existing CRISPR technology are mainly based on fluorescence[3] and immunochromatography.[14,15] The fluorescence method depends on the use of fluorescence readout equipment, which limits its widespread adoption and implementation in resource-constrained settings. The lateral flow assay can detect CRISPR cleavage products to generate visual results without the need for external equipment. However, two issues arise: the transfer of reaction products can lead to aerosol contamination, and colloidal gold exhibits a weak color signal and lower sensitivity compared with fluorescence detection methods.[16,17] Therefore, developing fully integrated CRISPR devices that can execute

Received: October 16, 2024
Revised: February 4, 2025
Accepted: February 6, 2025

Downloaded via SHANGHAI NORMAL UNIV on February 20, 2025 at 00:14:01 (UTC).
See https://pubs.acs.org/sharingguidelines for options on how to legitimately share published articles.

ACS Publications © XXXX American Chemical Society

Scheme a. Principle of Nanozyme-Catalyzed Colorimetric CRISPR Assay for Microfluidics Detection of Monkeypox Virus[a]



[a](i) Nucleic acids released from the monkeypox virus initiated the single-step RPA-CRISPR assay for trans-cleavage of FAM-ssRNA-Biotin reporters. (ii) ssRNA reporters were recognized by FAM antibody-conjugated GO@Pt nanozymes and streptavidin-coated magnetic beads. (iii) The sandwich immune complexes were blocked by a filter membrane and catalyzed the oxidation of the TMB substrate. The whole analysis procedure is integrated on a microfluidic chip

the whole analysis is necessary to eliminate the need for sophisticated equipment and the risk of aerosol contamination.

Various nanozymes with high catalytic ability have been widely developed and applied in the biosensing field for pathogen detection.[18,19] For example, a CeO_2 nanozyme-mediated RPA-CRISPR/Cas12a dual-mode biosensor was developed for the detection of the *invA* gene in *Salmonella*.[20] Current nanozymes, such as Fe_3O_4@Pt, Au−Ir, and Au@Pt NPs, predominantly exhibit a spherical structure.[19,21−23] Meanwhile, two-dimensional (2D) graphene materials possess a large specific surface area and high conductivity,[24,25] making them suitable for catalytic applications. Nanomaterial labels based on 2D graphene oxide have been verified with outstanding detection efficiency in the lateral flow assay detection of pathogens.[26,27]

Herein, a single-step RPA-CRISPR/Cas13a combined with a nanozyme-catalyzed colorimetric microfluidic platform was established for the highly sensitive visual detection of MPXV. An innovative graphene oxide (GO)-based 2D nanozyme with a high catalytic capacity was prepared. Numerous Au seeds were adsorbed for porous Pt shell deposition to prepare high-performance 2D nanozymes. The viral nucleic acids released from the clinical samples initiated a single-step RPA-CRISPR/Cas13a for the trans-cleavage of ssRNA reporters labeled with FAM and biotin, which can be recognized by FAM antibody-conjugated GO@Pt nanozymes and streptavidin-coated magnetic beads (MBs). The formed sandwich immunocomplexes can catalyze the oxidation of the colorless 3,3′,5,5′-tetramethylbenzidine (TMB) substrate with a distinct color change. A syringe-driven microfluidic chip was developed to fully accommodate the whole workflow, including single-step CRISPR, immune binding, filtration washing, and color rendering. This system exhibits an LOD of 1 copy/μL of MPXV DNA in 60 min. Its clinical feasibility was validated by testing rash fluid and oral swabs. The results are visible to the naked eye, demonstrating the system's potential applications in detecting monkeypox and other pathogens under resource-limited conditions.

EXPERIMENTAL SECTION

Preparation and Conjugation of GO@Pt. The preparation of Au seeds with a 3 nm diameter is presented in Section S1.3. 900 μL of GO solution (2 mg/mL) was added to 900 μL of deionized water and sonicated for 15 min to disperse completely. The mixture was then centrifuged for 8 min at

https://doi.org/10.1021/acs.analchem.4c05570
Anal. Chem. XXXX, XXX, XXX−XXX

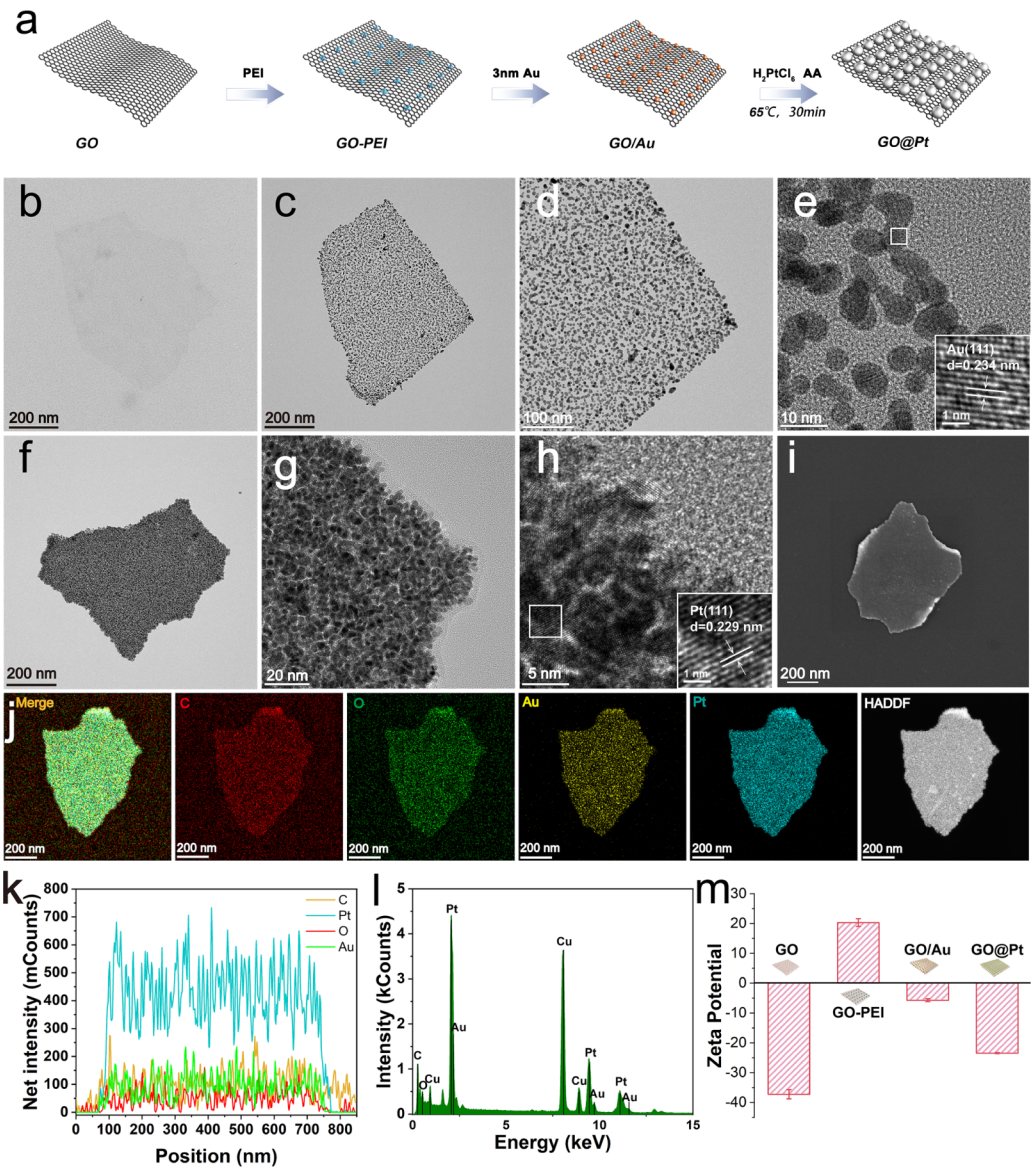


Figure 1. Preparation of two-dimensional GO@Pt nanozyme. (a) Schematic diagram of the synthesis of GO@Pt nanozyme. TEM images of (b) GO, and (c–e) GO/Au. (f–h) TEM images, and (i) SEM image of GO@Pt nanoflakes. (j) HAADF TEM image, (k) the corresponding EDS elemental line scan, and (l) the proportion of each element of GO@Pt. (m) Zeta potentials of GO, GO-PEI, GO@Au, and GO@Pt.

13800 rpm, and the sediment was resuspended in 900 μL of deionized water. Meanwhile, 500 μL of GO solution was added to 1 mL of deionized water and sonicated, followed by the addition of 200 μL of PEI and another sonication for 40 min. The mixture was then centrifuged for 10 min at 13800 rpm, washed twice, and the sediment was resuspended in 500 μL of deionized water. 80 mL of Au was added to 500 μL of the GO-PEI solution. The mixture was sonicated for 35 min and then centrifuged for 6 min at 6000 rpm. The precipitate was washed once with deionized water and then resuspended in 5 mL of anhydrous ethanol. Afterward, 400 μL of GO/Au nanosheet was centrifuged for 6 min at 6000 rpm and then resuspended in 800 μL of 0.4% (w/w) polyvinylpyrrolidone (PVP) solution. The product was added with 40 μL of ascorbic acid (AA) (100 mg/mL) for ultrasonic dispersion, followed by the dropwise addition of 40 μL of H_2PtCl_6 (100 mM) and incubation at 65 °C for 30 min. After the reaction, the products were centrifuged for 5 min at 5000 rpm, washed once with deionized water, and resuspended in 400 μL of anhydrous ethanol. The details of antibody modification of GO@Pt are presented in Section S1.4.

Development of a Single-Step RPA-CRISPR/Cas13a Assay. RPA primer and crRNA sequences were designed with Primer Premier 5 to obtain high reaction efficiency. The details are displayed in Table S1. The details of the preparation of crRNA are presented in Section S1.5. In brief, 70 μL of master mix was prepared with 1× RPA rehydration buffer, 50 nM LwaCas13a, 1 U/μL of T7 RNA polymerase, 1 U/μL of RNase H, 2.5 U/μL of RNase inhibitor, 1 μM FAM-UUUUU-Biotin, 4 mM rNTP mix, and 250 nM forward primer: MPXV-RPA-F1, 250 nM reverse primer: MPXV-RPA-R4, and 500 nM transcriptional crRNA: MPXV-crRNA2. Then, 5 μL of MPXV DNA target (Figure S1) and 1 μL of magnesium acetate (280 mM) were added to 14 μL of master mix. The mixture was transferred to the reaction chamber of the microfluidic chip to obtain a 37 °C reaction condition.

Design and Fabrication of Microfluidic Chip. The microfluidic chip was designed using SOLIDWORKS 2017

https://doi.org/10.1021/acs.analchem.4c05570
Anal. Chem. XXXX, XXX, XXX−XXX

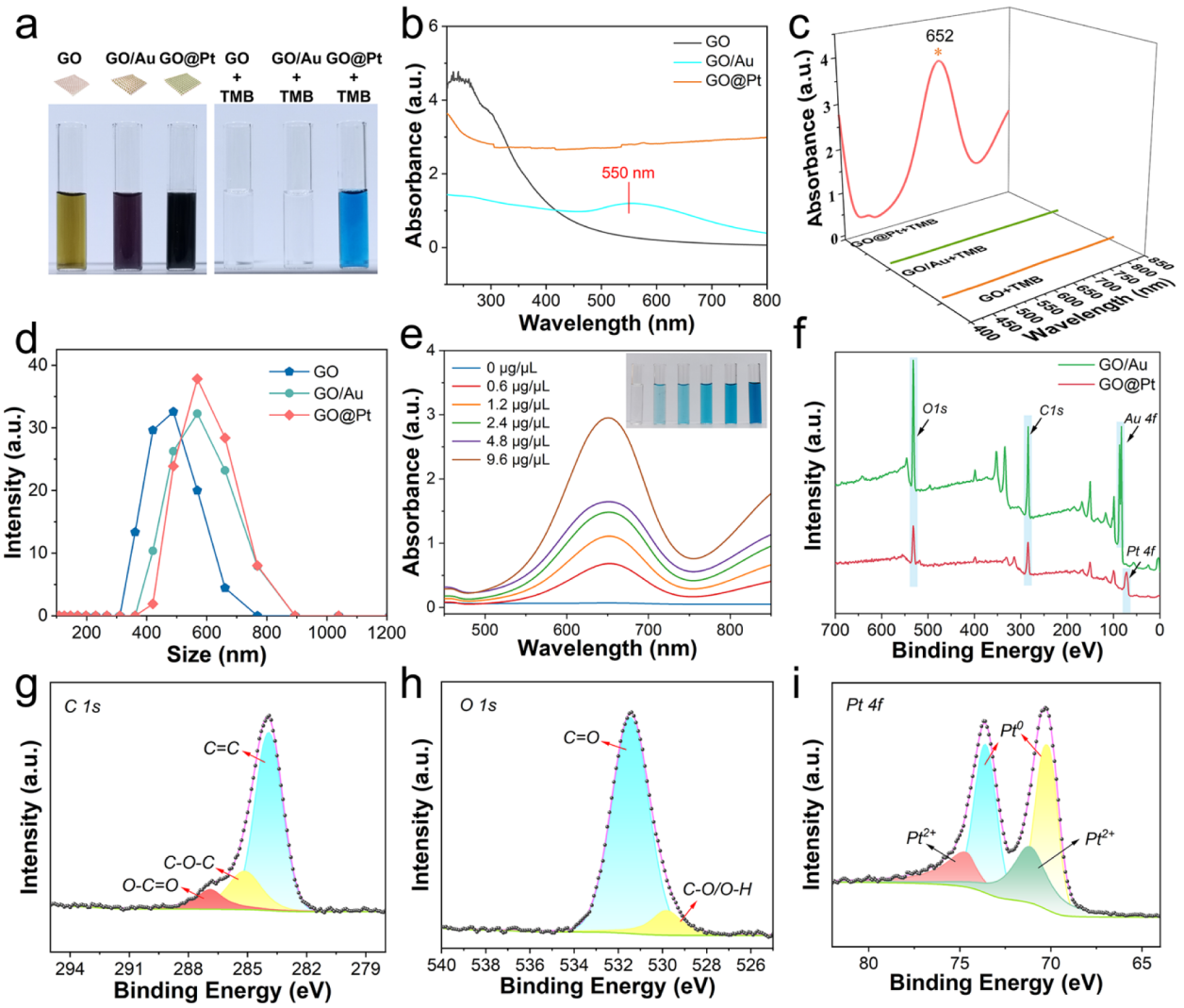


Figure 2. Characterization of two-dimensional GO@Pt nanozyme. (a) Photographs, and (b−c) UV−vis spectra of GO, GO/Au, GO@Pt, and their mixtures with TMB substrate. (d) Dynamic light scattering distribution of GO, GO/Au, GO@Pt. (e) UV−vis spectra of TMB substrate catalyzed by different concentrations of GO@Pt nanozyme. (f) Wide-scan XPS spectra, and (g) C 1*s*, (h) O 1*s*, and (i) Pt 4*f* spectra of GO@Pt nanozyme.

and composed of five layers from bottom to top, including the bottom-sealing pressure-sensitive adhesive (PSA), filter membrane (pore size of 2 μm), main structure of the microfluidic chip, top-sealing PSA, and PDMS gasket. The size of the microfluidic chip was 75 × 25 × 4 mm^3, and the chip was manufactured with poly(methyl methacrylate) (PMMA). The microfluidic chip was composed of a sample inlet, a buffer inlet, a CRISPR reaction chamber, a nanomaterial storage chamber, an incubation chamber, a filter membrane (aperture 2 μm), a color rendering chamber, a PDMS grommet, a medical syringe, upper and lower PSAs of corresponding size, and a microchannel connecting the various components.

On-Chip Nanozyme-Catalyzed Colorimetric CRISPR Assay. Clinical samples were mixed with a lysis buffer (20% Chelex-100, 50 mM TCEP in TE buffer (10 mM Tris, 1 mM EDTA (pH 8.0))) at a ratio of 1:9. The mixture was heated at 80 °C for 2 min to release viral nucleic acid. Then, 5 μL of virus lysis, 1 μL of magnesium acetate, and 14 μL of the RPA-CRISPR master mix were introduced into the CRISPR reaction chamber via the sample inlet. The microfluidic chip was incubated at 37 °C for 30 min. Subsequently, FAM antibody-conjugated GO@Pt nanozymes and streptavidin-coated MBs in 100 μL of buffer (10 mM PBS, 0.05% Tween-20, 1 wt % BSA) were added via the reagent inlet. The CRISPR mixture and reagents were incubated for 15 min in the chamber, and the formed sandwich immune complexes in the resultant mixture flowed through the filter membrane under the driving of a syringe. Finally, 50 μL of TMB was added after three washes with 100 μL of buffer and left for color development for 15 min.

RESULTS AND DISCUSSION

Principle of 2D Nanozyme-Catalyzed Colorimetric CRISPR Assay for MPXV Detection. Herein, we demonstrate a 2D nanozyme-catalyzed colorimetric CRISPR assay for MPXV detection on an integrated microfluidic chip. As shown in Scheme a, the collected rash fluid swabs and oral swabs are treated with extraction-free viral lysis for 2 min at 80 °C, followed by a single-step RPA-CRISPR/Cas13a reaction for 30 min at 37 °C. The target nucleic acid sequence is identified specifically by Cas13a and crRNA complexes, which can trans-cleave the nonspecific RNA reporter group. After cutting, the probe is incubated with nanozyme and MBs for 15 min and then eluted three times. The GO@Pt nanozyme, MBs, and

https://doi.org/10.1021/acs.analchem.4c05570
Anal. Chem. XXXX, XXX, XXX−XXX

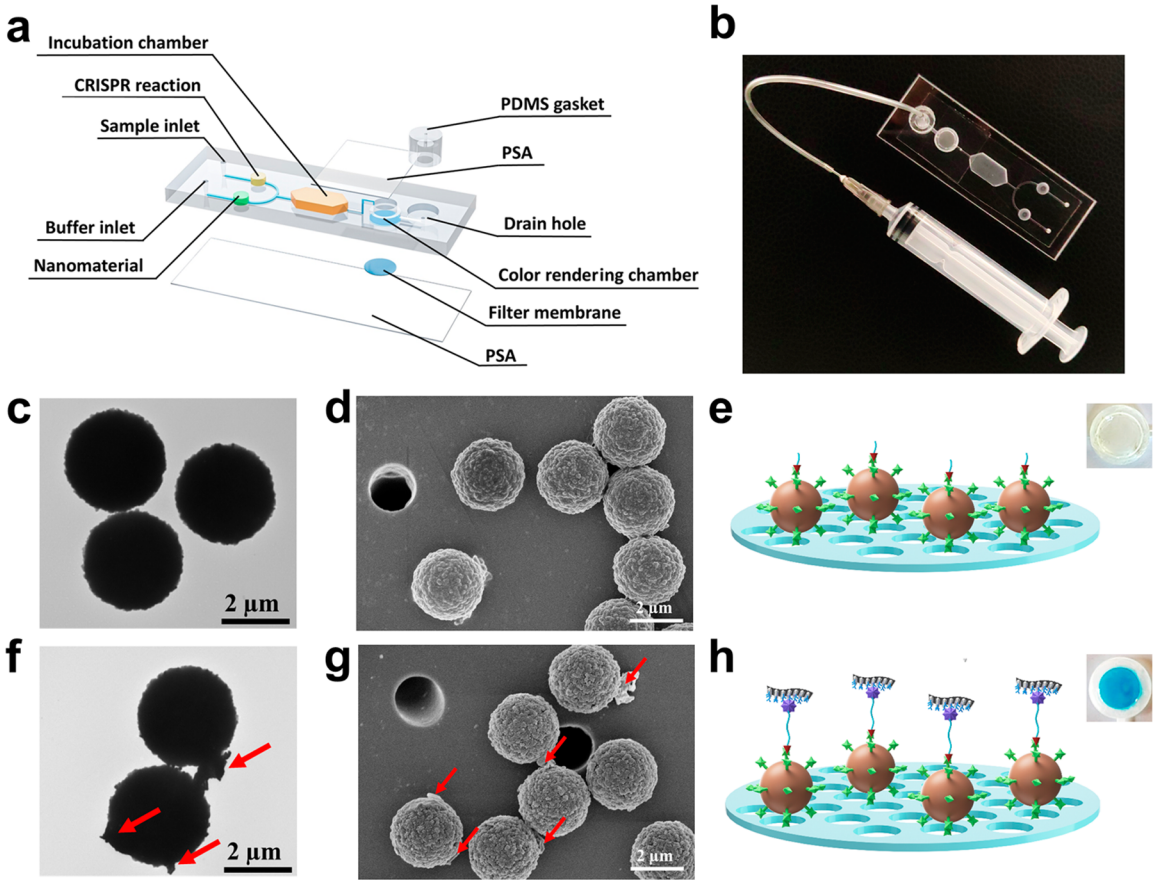


Figure 3. Design of microfluidic chip for nanozyme-catalyzed colorimetric CRISPR assay. (a) Schematic diagram and (b) photograph of the designed microfluidic chip. (c) TEM image, (d) SEM image, and (e) schematic illustration of magnetic beads without nanozymes for positive testing. Inset of (e): Photograph of resultant color rendering chamber for positive testing. (f) TEM image, (g) SEM image, and (h) schematic illustration of magnetic beads with captured nanozymes for negative testing. Inset of (h): Photograph of resultant color rendering chamber for negative testing.

ssRNA reporter are combined as a complex structure. The size of the MB is 2.8 μm, and that of the GO@Pt is approximately 1 μm. Thus, we selected a 2 μm filter membrane for experiments to filter out the GO@Pt nanozyme and other small-sized reactants, leaving the MBs and MB−probe−nanozyme complex on the filter membrane. Finally, TMB is added for color development for 15 min, and the solution turns blue for accurate and efficient detection of the target DNA. The entire experimental process, including sample lysis, nucleic acid amplification, system incubation and cleaning, and color development reaction, is carried out on a microfluidic chip. Our proposed CRISPR/Cas13a detection system based on nanozyme can realize accurate molecular diagnostics in 60 min for MPXV detection under limited resources.

Characterization of GO@Pt Nanozyme. The structure and chemical properties of the synthesized GO@Pt nanozyme are characterized in detail. As shown in Figure 1a, a layer of PEI molecules was coated on the surface of GO to adsorb 3 nm Au seeds for Pt shell deposition. As displayed in the transmission electron microscopy (TEM) image in Figure 1b, the individual GO nanosheet appears as a translucent film. After the adsorption of GO nanosheets on PEI, the potential rapidly increases from −37.23 to +20.28 mV, suggesting that PEI is successfully adsorbed onto the surface of GO nanosheets (Figure 1m). As the Au nanoparticles are adsorbed, the electrode potential of the GO/Au nanoflakes gradually decreases to −5.71 mV (Figure 1m). Figure 1c,d shows that the Au nanoparticles are uniformly dispersed on the surface of the GO-PEI nanoflakes. The HRTEM image in Figure 1e displays that the interplanar spacing of the adsorbed Au nanoparticles is 0.234 nm, which can be attributed to the cubic structure of the Au (111) nanoparticles plane. Figure 1f exhibits the morphology of a single GO@Pt nanoparticle. The enlarged GO@Pt nanosheet displays a continuous growth of dense Pt nanoparticles on its surface (Figure 1g). The lattice spacing of deposited Pt nanoparticles is 0.229 nm (Figure 1h), which may be due to the cubic structure of the Pt nanoparticle (111) plane. Similarly, Figure 1i indicates that continuous and dense Pt shells are grown on the surfaces of GO@Pt nanosheets. As the Pt grows, it gradually fills the exposed areas of the PEI, and the potential of GO@Pt continues to decrease to −23.44 mV (Figure 1m). Energy-dispersive spectroscopy (EDS) and high-angle annular dark-field (HAADF) TEM image (Figure 1j) show the element distribution of individual GO@Pt nanosheet, with Pt (blue) evenly distributed in the outer layers of GO/Au nanosheets with C (red), O (green), and Au (yellow). The EDS line scanning result in Figure 1k also verifies that Pt is evenly distributed in the outer layer of the GO/Au nanosheets. EDS dot scanning reveals C, O, Au, and Pt signals (Figure 1l) in the GO@Pt nanostructures.

https://doi.org/10.1021/acs.analchem.4c05570
Anal. Chem. XXXX, XXX, XXX−XXX

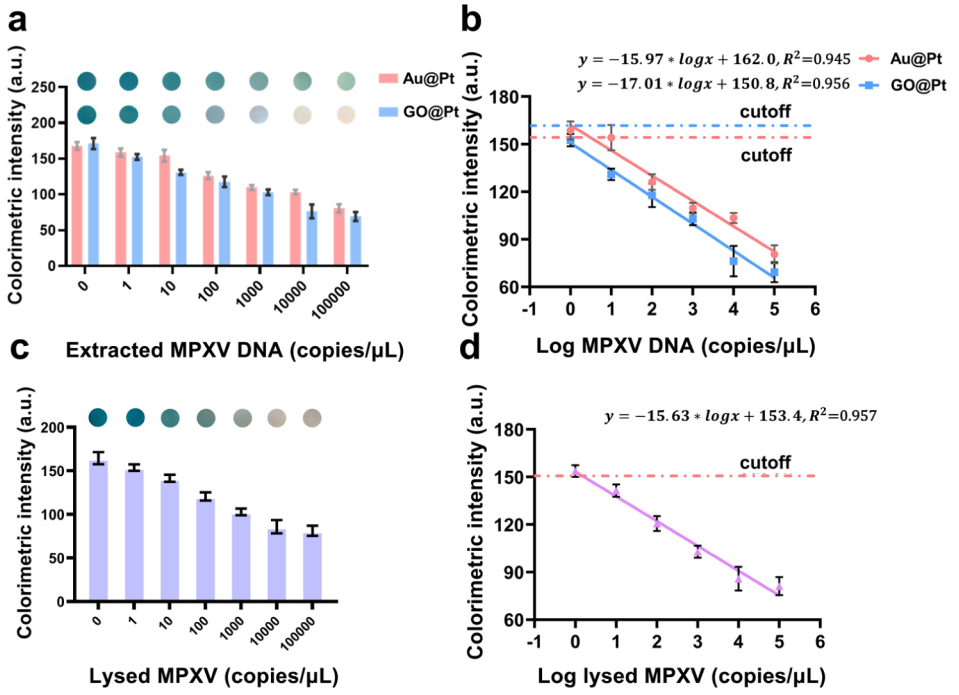


Figure 4. Analytical performance of nanozyme-catalyzed colorimetric CRISPR assay for MPXV detection. (a) Photographs, colorimetric signals, and (b) the linear fitting curves of GO@Pt and Au@Pt catalyzed colorimetric CRISPR microfluidic assays for extracted MPXV DNA at the different concentrations. (c) Photographs, colorimetric signals, and (d) the linear fitting curve of GO@Pt catalyzed colorimetric CRISPR microfluidic assay for lysed MPXV at different concentrations. Error bar represents standard deviation of three repetitive experiments.

The catalytic performances of GO, GO/Au, and GO@Pt on the TMB substrate are further verified. The mixture of GO@Pt and TMB changes to blue, while both GO and GO/Au remain colorless after mixing with TMB (Figure 2a). This color rendering suggests that only GO@Pt can catalyze the TMB substrate. Meanwhile, we examine the absorption of GO, GO/Au, and GO@Pt before and after TMB addition (Figure 2b,c). Only the absorption of GO@Pt shifts to 625 nm after TMB addition, and the other nanomaterials have no obvious absorption. GO@Pt greatly accelerates the oxidation of TMB to ox-TMB and thus can be an effective nanozyme; this ability is primarily contributed by the in situ reduced Pt NPs. Figure 2d represents the diameter of GO (300−700 nm), GO/Au (400−800 nm), and GO@Pt (400−800 nm). As indicated in Figure 2e, the absorbance intensity at 625 nm increases with the concentration of GO@Pt from 0 to 9.6 μg/μL. The GO@Pt nanozyme with a concentration of 9.6 μg/μL shows the deepest color and thus the strongest catalytic capacity. The typical peaks of O, C, and Au 4*f* for GO/Au and O, C, and Pt 4*f* for GO@Pt appear in the XPS spectra in Figure 2f. Moreover, the high-resolution XPS spectra of C 1*s* (C═C, C−O−C, and O—C═O), O 1*s* (C═O, C−O/O−H), and Pt 4*f* (Pt^{2+}, Pt^0) are carried out as shown in Figure 2g−i. All of the above results confirm the successful decoration of Pt NPs on GO/Au nanosheets. As depicted in Figure S2a,b, the GO@Pt nanozyme demonstrates outstanding colloidal stability and colorimetric signal stability in highly saline solutions and the pH range of 1−14. In addition, the colorimetric signal of GO@Pt remains stable in the composite sample, and the colloidal stability and colorimetric signal of GO@Pt do not remarkably change after being stored in dark conditions for 1−6 months (Figure S2c). These outcomes reveal that the fabricated GO@Pt nanozyme flawlessly integrates the stability and dispersibility of GO nanosheets with the exceptional colorimetric properties of Pt NPs. Such properties endow them with considerable potential to supplant ordinary spherical nanozymes as high-performance nanotags.

Single-Step RPA-CRISPR/Cas13a Assay. Four pairs of primers and three crRNAs (Table S1) were designed for the experiments, and the optimal combination of primers and crRNA for single-step CRISPR was determined (Figure S3). To verify the target-triggered trans-cleavage of CRISPR/Cas13a, MPXV nucleic acid templates were amplified and transcribed into the RNA target. Purified RNA target was added with or without Cas13a protein. The real-time fluorescence curve for the group with Cas13a in Figure S4 shows a positive signal, which verified the target-triggered trans-cleavage of CRISPR/Cas13a. Several important reaction conditions of RPA-CRISPR/Cas13a, such as primer concentration, rNTP mix, RNase H, T7 RNA polymerase, crRNA, and Cas13a, were optimized. Figure S5 shows the optimized conditions of 250 nM primer, 4 mM rNTP mix, 1 U/μL RNase H, 1 U/μL T7 RNA polymerase, 0.5 μM crRNA, and 0.5 nM Cas13a. Subsequent detection experiments were carried out under these optimized conditions.

Design and Fabrication of Microfluidic Chip. As shown in Figure 3a, the main structure of the microfluidic chip consists of a sample inlet, buffer inlet, CRISPR reaction chamber (25 μL), nanomaterial chamber (25 μL), incubation chamber (180 μL), color-rendering chamber, drain hole, and microchannel. In this structure, the sample and buffer enter from two separate inlets, and the CRISPR reaction chamber offers a relatively independent reaction space for RPA-CRISPR/Cas13a detection. The nanomaterial storage chamber is utilized to store immunomagnetic beads and functionalized 2D nanozyme, and the incubation chamber provides a space for the probe, immunomagnetic beads, and functionalized 2D nanocatalytic signal tags to bind and form immune complexes.

https://doi.org/10.1021/acs.analchem.4c05570
Anal. Chem. XXXX, XXX, XXX−XXX

The filter membrane enriches the complexes and has a color display window on top for signal intensity. A medical syringe offers the driving force for the entire process. Figure 3b shows the physical image of the microfluidic chip. To verify the accuracy of 2D nanozyme-catalyzed colorimetric CRISPR for the microfluidic detection of MPXV, we selected 10^5 copies/μL MPXV positive samples and negative samples for testing. The positive and negative reactions are characterized by TEM and SEM. Figure 3c exhibits a positive outcome with MBs, suggesting that the CRISPR reaction cleaves the probe and prevents the MB−probe−nanozyme from binding. The SEM image in Figure 3d indicates that MBs are successfully stuck on the filter membrane. The TMB substrate cannot catalyze the MBs without the nanozyme; thus, the filter color does not change to blue (Figure 3e). The negative result is displayed in Figure 3f, with MB, probe, and GO@Pt nanozyme forming a complex. The flexible 2D GO@Pt nanozyme is tightly attached to MB. After being eluted three times, the dissociative nanozyme and other micromolecules are washed off, and the formed complex remains on the filter membrane (Figure 3g). The complex catalyzes the TMB substrate into a blue color (Figure 3h).

Optimization of Nanozyme-Catalyzed Colorimetric CRISPR Assay. The synthesis parameters of the GO@Pt nanozymes are optimized by adding varying amounts of GO/Au seeds. As depicted in Figure S6, 400 μL of GO/Au exhibits the most excellent color rendering effect and the optimal colorimetric outcomes. Several vital experimental conditions, including the amount of nanozyme, amount of MBs, amount of ssRNA reporter, color rendering time, and incubation time, are also optimized to achieve the best response to the detection system. As shown in Figures S7a−e, 5 μL of MBs, 15 μL of nanozymes, 1.5 μM ssRNA reporters, 15 min of color development time, and 15 min of incubation time are selected as the most appropriate.

Analytical Performance of Nanozyme-Catalyzed Colorimetric CRISPR Assay. The cultured MPXV quantified by digital PCR is applied as a reference standard to determine the LOD. As shown in Figure 4a, the as-synthesized GO@Pt and a widely used Au@Pt nanozyme are applied to evaluate the LODs for MPXV detection. The details of the synthesis and characteristics of Au@Pt are provided in Figure S8. The colorimetric signals of the testing results for these two assays weaken with the increase in target MPXV DNA templates, and the signal weakening trend is more evident for the GO@Pt-catalyzed assay. As shown in Figure 4b, the signal intensities of GO@Pt-catalyzed and Au@Pt-catalyzed colorimetric CRISPR microfluidic assays exhibit a wide dynamic linear range with R^2 values of 0.956 and 0.945, respectively. Based on the signal-to-noise ratio, the detection thresholds of GO@Pt and Au@Pt assays are determined as 159.98 and 154.08, respectively. The LODs for GO@Pt- and Au@Pt-catalyzed colorimetric CRISPR assays are 1 and 10 copies/μL of MPXV DNA template, respectively. Thus, the GO@Pt nanozyme-catalyzed CRISPR assay is more sensitive than the Au@Pt-catalyzed assay. This improvement can be attributed to the large surface area and porous nanostructure of GO@Pt as a 2D flexible nanozyme, facilitating the capture of the target analyte and significantly increasing the catalytic capability. A direct lysis of MPXV comparison is also conducted. Figure 4c−d shows that the LOD is also 1 copy/μL of lysed MPXV, which is consistent with the LOD for extracted nucleic acid template. Table S2 summarizes the analytical performances of currently existing CRISPR-based assays for MPXV detection, including amplification-free CRISPR/Cas12a,[6] DNAzyme-based chemiluminescence CRISPR/Cas12a,[28] two-step RPA-CRISPR/Cas12a,[1,29,30] single-step RPA-CRISPR/Cas12a,[31] and single-step RPA-CRISPR/Cas13a.[32] The proposed nanozyme-catalyzed RPA-CRISPR/Cas13a assay is simple to use and user-friendly because of its streamlined viral lysis and colorimetric readout by the naked eye on an integrated microfluidic chip. Furthermore, it can achieve superior assay sensitivity to most CRISPR assays in resource-limited settings since it does not require any benchtop instruments for sample pretreatment, fluidic control, and fluorescence readout.

Figure S9 shows that VTT and VZV, similar to MPXV, are selected to verify specific detection. The results show that the detection system has excellent specificity. Three different concentrations of MPXV (0, 10, and 10000 copies/μL) are then tested to verify the stability of the diagnostic system. As shown in Figure S10, the coefficient of variation for 0, 10, and 10000 copies/μL of MPXV is 5.16%, 6.48%, and 13.62%, respectively, demonstrating that this experiment has excellent repeatability and stability.

Application in Clinical Samples. Although numerous clinical simulated samples or pseudoviruses have been employed to develop CRISPR-based MPXV assays,[6,31,33] the validation of sensitivity and specificity through actual clinical MPXV samples is restricted. The performance of our detection method must be assessed in real-world scenarios to guarantee its reliability and suitability. In this study, 40 clinical samples, including rash fluid swabs (11 negative and 9 positive samples) and oral swabs (11 negative and 9 positive samples), are collected to verify the clinical feasibility of this proposed assay. First, we detect the 40 clinical samples via a real-time fluorescence PCR assay (Figure S11). The detection results are shown in Figure 5a, and the cycle threshold (Ct) values of 9 positive rash fluid swab samples and 9 positive oral swabs range from 11.9 to 27.7 and 27.3 to 36.2, respectively. Meanwhile, the negative samples exhibit no Ct values. The photographs and colorimetric signal intensities obtained using the proposed method for the 40 clinical samples are shown in Figure 5b,c. The receiver-operating characteristic curve for the proposed method is plotted in Figure 5d with an area under the curve of 1, suggesting that this detection system can correctly identify all 40 clinical samples with 100% sensitivity and 100% specificity. The PCR Ct values of the positive samples range from 11.9 to 36.2, which are 100% consistent with the detection system in all clinical samples (Figure 5e). This finding indicates that the proposed method for MPXV detection has a competitive detection performance compared with the gold standard PCR. This diagnostic system possesses superior diagnostic accuracy and holds great potential for clinical application.

CONCLUSIONS

We developed a highly sensitive 2D nanozyme-catalyzed colorimetric CRISPR assay for MPXV detection on an integrated microfluidic chip. The synthesized 2D GO@Pt nanozymes possess a large surface area, porous structure, and expanded reaction area, which are utilized as the label with excellent peroxidase-like catalytic activity. The viral nucleic acids released from clinical samples initiate a single-step RPA-CRISPR/Cas13a for the trans-cleavage of FAM-ssRNA-biotin reporters, which can be recognized by FAM antibody-conjugated GO@Pt nanozymes and streptavidin-coated MBs.

https://doi.org/10.1021/acs.analchem.4c05570
Anal. Chem. XXXX, XXX, XXX−XXX

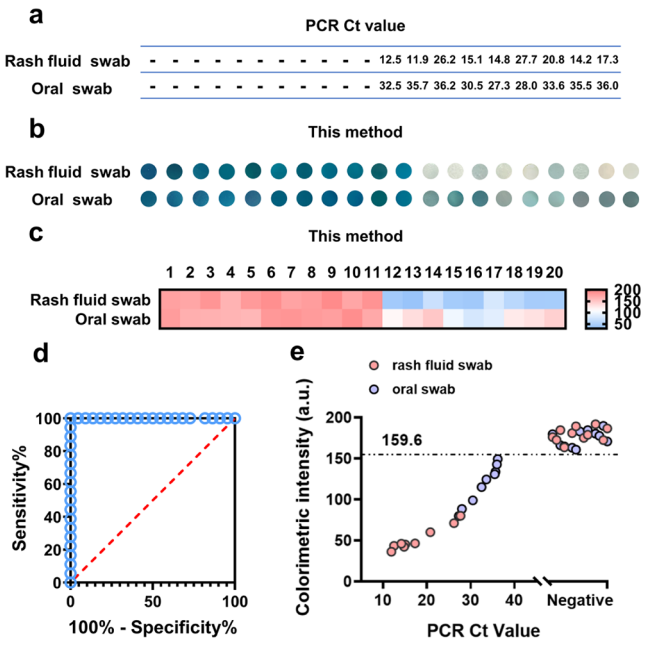


Figure 5. Analysis of clinical samples by using GO@Pt nanozyme-catalyzed colorimetric CRISPR assay. (a) The qPCR Ct values of monkeypox virus nucleic acid in clinical samples. (b–c) The photographs and colorimetric intensities of GO@Pt nanozyme-catalyzed colorimetric CRISPR assay for clinical samples. (d) The receiver-operating characteristic curve. (e) Clinical sample PCR Ct value plotted against colorimetric intensity of this assay.

The formed sandwich immunocomplexes can catalyze the oxidation of the colorless TMB substrate with a distinct color change. The designed syringe-driven microfluidic chip fully accommodates the whole workflow under the guidance of a medical syringe. The proposed GO@Pt-catalyzed colorimetric CRISPR assay exhibited an LOD of 1 copy/μL of MPXV in 60 min. Forty clinical samples were validated, and the results were 100% in agreement with the real-time fluorescence PCR. The on-chip colorimetric CRISPR assay achieves accurate molecular diagnostics with naked eye readout that eliminates aerosol contamination risk and the need for specialized instruments. Owing to its simple-to-use format and superior analytical performance, this assay holds great potential for the sensitive and accurate point-of-care testing of infectious pathogens under resource-limited settings.

■ ASSOCIATED CONTENT

Supporting Information

The Supporting Information is available free of charge at https://pubs.acs.org/doi/10.1021/acs.analchem.4c05570.

Digital PCR for quantification of monkeypox virus, stability of GO@Pt nanozyme, primers and crRNAs screening, verification of the target-triggered trans-cleavage of CRISPR/Cas13a, optimization of CRISPR/Cas13a and GO@Pt, synthesis and characterization of Au@Pt nanozymes, specificity and repeatability of this diagnostic system, clinical sample detection via qPCR, the sequences of primers and CRISPR crRNA, and comparison of assay performances (PDF)

■ AUTHOR INFORMATION

Corresponding Authors

Rui Song − *Beijing Ditan Hospital, Capital Medical University, Beijing 100015, China*; Email: songruii@hotmail.com

Shengqi Wang − *Bioinformatics Center of AMMS, Beijing 100850, China; State Key Laboratory of Kidney Diseases, Beijing 100853, PR China*; Email: sqwang@bmi.ac.cn

Zhen Rong − *Bioinformatics Center of AMMS, Beijing 100850, China*; orcid.org/0000-0001-7111-0504; Email: rongzhen0525@sina.com

Authors

Hong Chen − *Bioinformatics Center of AMMS, Beijing 100850, China*

Xiaodan Cheng − *Bioinformatics Center of AMMS, Beijing 100850, China*

Yunxiang Wang − *Bioinformatics Center of AMMS, Beijing 100850, China*

Ning Han − *Beijing Ditan Hospital, Capital Medical University, Beijing 100015, China*

Liyan Liu − *Bioinformatics Center of AMMS, Beijing 100850, China*

Hongjuan Wei − *Bioinformatics Center of AMMS, Beijing 100850, China*

Zhijie Tu − *Bioinformatics Center of AMMS, Beijing 100850, China*

Zhixia Gu − *Beijing Ditan Hospital, Capital Medical University, Beijing 100015, China*

Complete contact information is available at: https://pubs.acs.org/10.1021/acs.analchem.4c05570

Author Contributions

#H.C., X.C., Y.W., and N.H. contributed equally to this work.

Notes

The authors declare no competing financial interest.

■ REFERENCES

(1) Low, S. J.; O'Neill, M. T.; Kerry, W. J.; Krysiak, M.; Papadakis, G.; Whitehead, L. W.; Savic, I.; Prestedge, J.; Williams, L.; Cooney, J. P.; Tran, T.; Lim, C. K.; Caly, L.; Towns, J. M.; Bradshaw, C. S.; Fairley, C.; Chow, E. P. F.; Chen, M. Y.; Pellegrini, M.; Pasricha, S.; Williamson, D. A. *Lancet Microbe* **2023**, *4* (10), No. e800−e810.

(2) Sitaula, C.; Shahi, T. B. *J. Med. Syst.* **2022**, *46* (11), 78.

(3) Fu, X.; Sun, J.; Ye, Y.; Zhang, Y.; Sun, X. *Biosens. Bioelectron.* **2022**, *195*, 113682.

(4) Huang, M.; Zhou, X.; Wang, H.; Xing, D. *Anal. Chem.* **2018**, *90* (3), 2193−2200.

(5) Huang, X.; Zhang, F.; Zhu, K.; Lin, W.; Ma, W. *Virus Res.* **2021**, *304*, 198530.

(6) Chen, Y.; Chen, Z.; Li, T.; Qiu, M.; Zhang, J.; Wang, Y.; Yuan, W.; Ho, A. H.-P.; Al-Hartomy, O.; Wageh, S.; Al-Sehemi, A. G.; Shi, X.; Li, J.; Xie, Z.; Xuejin, L.; Zhang, H. *ACS Nano* **2023**, *17* (13), 12903−12914.

(7) Maksyutov, R. A.; Gavrilova, E. V.; Shchelkunov, S. N. *J. Virol. Methods* **2016**, *236*, 215−220.

(8) Chen, J. S.; Ma, E.; Harrington, L. B.; Da Costa, M.; Tian, X.; Palefsky, J. M.; Doudna, J. A. *Science* **2018**, *360* (6387), 436−439.

(9) Teng, F.; Guo, L.; Cui, T.; Wang, X.-G.; Xu, K.; Gao, Q.; Zhou, Q.; Li, W. *Genome Biol.* **2019**, *20* (1), 132.

(10) Zeng, R.; Gong, H.; Li, Y.; Li, Y.; Lin, W.; Tang, D.; Knopp, D. *Anal. Chem.* **2022**, *94* (20), 7442−7448.

(11) Nguyen, L. T.; Smith, B. M.; Jain, P. K. *Nat. Commun.* **2020**, *11* (1), 4906.

(12) Yang, Y.; Gong, F.; Shan, X.; Tan, Z.; Zhou, F.; Ji, X.; Xiang, M.; Wang, F.; He, Z. *Microchim. Acta* **2024**, *191* (2), 102.
(13) Ahamed, M. A.; Khalid, M. A. U.; Dong, M.; Politza, A. J.; Zhang, Z.; Kshirsagar, A.; Liu, T.; Guan, W. *Biosens. Bioelectron.* **2024**, *246*, 115866.
(14) Ali, Z.; Sanchez, E.; Tehseen, M.; Mahas, A.; Marsic, T.; Aman, R.; Sivakrishna Rao, G.; Alhamlan, F. S.; Alsanea, M. S.; Al-Qahtani, A. A.; Hamdan, S.; Mahfouz, M. *ACS Synth. Biol.* **2022**, *11* (1), 406−419.
(15) Choi, J. H.; Lim, J.; Shin, M.; Paek, S. H.; Choi, J. W. *Nano Lett.* **2021**, *21* (1), 693−699.
(16) Arizti-Sanz, J.; Freije, C. A.; Stanton, A. C.; Petros, B. A.; Boehm, C. K.; Siddiqui, S.; Shaw, B. M.; Adams, G.; Kosoko-Thoroddsen, T.-S. F.; Kemball, M. E.; et al. *Nat. Commun.* **2020**, *11* (1), 5921.
(17) Xiong, E.; Jiang, L.; Tian, T.; Hu, M.; Yue, H.; Huang, M.; Lin, W.; Jiang, Y.; Zhu, D.; Zhou, X. *Angew. Chem. Int. Ed.* **2021**, *60* (10), 5307−5315.
(18) Bai, T.; Wang, L.; Wang, M.; Zhu, Y.; Li, W.; Guo, Z.; Zhang, Y. *Biosens. Bioelectron.* **2022**, *208*, 114218.
(19) Broto, M.; Kaminski, M. M.; Adrianus, C.; Kim, N.; Greensmith, R.; Dissanayake-Perera, S.; Schubert, A. J.; Tan, X.; Kim, H.; Dighe, A. S.; Collins, J. J.; Stevens, M. M. *Nat. Nanotechnol.* **2022**, *17* (10), 1120−1126.
(20) Arshad, F.; Abdillah, A. N.; Shivanand, P.; Ahmed, M. U. *Biosens. Bioelectron.* **2024**, *247*, 115940.
(21) Zheng, C.; Jiang, Q.; Wang, K.; Li, T.; Zheng, W.; Cheng, Y.; Ning, Q.; Cui, D. *Analyst* **2022**, *147* (8), 1678−1687.
(22) Wei, Z.; Luciano, K.; Xia, X. *ACS Nano* **2022**, *16* (12), 21609−21617.
(23) Gao, Z.; Ye, H.; Tang, D.; Tao, J.; Habibi, S.; Minerick, A.; Tang, D.; Xia, X. *Nano Lett.* **2017**, *17* (9), 5572−5579.
(24) Shen, W.; Wang, C.; Zheng, S.; Jiang, B.; Li, J.; Pang, Y.; Wang, C.; Hao, R.; Xiao, R. *J. Hazard. Mater.* **2022**, *437*, 129347.
(25) Morales-Narváez, E.; Baptista-Pires, L.; Zamora-Gálvez, A.; Merkoçi, A. *Adv. Mater.* **2017**, *29* (7), 1604905.
(26) Cheng, X.; Yang, X.; Tu, Z.; Rong, Z.; Wang, C.; Wang, S. *J. Hazard. Mater.* **2023**, *459*, 132192.
(27) Cheng, X.; Zheng, S.; Wang, W.; Han, H.; Yang, X.; Shen, W.; Wang, C.; Wang, S. *Chem. Eng. J.* **2021**, *426*, 131836.
(28) Chen, H.; Feng, Y.; Liu, F.; Tan, C.; Xu, N.; Jiang, Y.; Tan, Y. *Biosens. Bioelectron.* **2024**, *247*, 115929.
(29) Gong, L.; Chen, X.; Wang, Y.; Liang, J.; Liu, X.; Wang, Y. *Front Public Health* **2023**, *11*, 1137968.
(30) Chen, Q.; Gul, I.; Liu, C.; Lei, Z.; Li, X.; Raheem, M. A.; He, Q.; Haihui, Z.; Leeansyah, E.; Zhang, C. Y.; Pandey, V.; Du, K.; Qin, P. *J. Med. Virol.* **2023**, *95* (1), No. e28385.
(31) Wei, J.; Wang, W.; Yu, Q.; Zhang, M.; Xue, F.; Fan, B.; Zhang, T.; Gao, Y.; Li, J.; Meng, X.; Pang, B. *Sens. Actuators, B* **2023**, *390*, 133950.
(32) Wang, Y.; Chen, H.; Lin, K.; Han, Y.; Gu, Z.; Wei, H.; Mu, K.; Wang, D.; Liu, L.; Jin, R.; Song, R.; Rong, Z.; Wang, S. *Nat. Commun.* **2024**, *15* (1), 3279.
(33) Wang, X.; Deng, X.; Zhang, Y.; Dong, W.; Rao, Q.; Huang, Q.; Tang, F.; Shen, R.; Xu, H.; Jin, Z.; Tang, Y.; Du, D. *Biosens. Bioelectron.* **2024**, *257*, 116268.

https://doi.org/10.1021/acs.analchem.4c05570
Anal. Chem. XXXX, XXX, XXX−XXX